



Report on single and double “shadow” junctions with ballistic transport

Author	Affiliation	Email
Jesper Nygård	UCPH	nygard@nbi.ku.dk
Project Number	Project Start Date	Duration
828948	01.04.2019	48 Months
Classification	PU	
File Name		
AndQC_deliverable_1.4.docx		
WP No	Work Package Name	
1	Material developments	
Deliverable No	Deliverable Name	
4	Single and double “shadow” junctions with ballistic transport	
Approved by		



The opinions expressed in the document are of the authors only and no way reflect the European Commission’s opinions. The European Union is not liable for any use that may be made of the information. This project has received funding from the European Union's Horizon 2020 research and innovation programme under grant agreement No 828948.

DOCUMENT REVISION HISTORY

Revision	Date	Description	Author
1.0	2.9.2021	AndQC_deliverable_1.4_TK_JN.docx	T. Kanne and J. Nygård
1.1	24.9.2021	AndQC_deliverable_draft.docx	T. Kanne, J. Nygård, J. Hinnerk and C. Schoenberg
1.2	29.9.2021	AndQC_deliverable_1.4_final.docx	T. Kanne, K. Grove-Rasmussen and J. Nygård

Table of Contents

1. Introduction	3
2. Fabrication of resist-less junctions.....	3
3. Electrical characterization of few-mode junctions.....	6
4. Implementation of superconducting junctions in cavities.....	8
5. Conclusion.....	10

1. Introduction

Conductance in InAs nanowires is notorious for being highly surface dependent due to intrinsic accumulation of charges at the surface. Because of this, ohmic contacts are easy achievable, but this also implies that the carrier mobility is particularly dependent on the chemical cleanliness and structural conformity of the surface. By in-situ evaporating thin Al shells on InAs nanowires, the Al films have been found to take specific bi-crystal interfacial matches relative to the underlying crystallographic basics of the InAs nanowire facets [Krogstrup (2015)]. Transport measurements utilizing these hybrid materials showed so-called hard gap induced superconductivity in the hybrid density of states, with absence of a continuum of subgap quasiparticle states [Chang (2015)]. The target of this deliverable is to demonstrate fabrication of single and double Josephson junctions in hybrid nanowires by using resist-less patterning of the superconductor and to show signs of ballistic transport in such shadow defined junctions.

2. Fabrication of resist-less junctions

Different strategies have been tested in order to fabricate resist-less junctions in metal films, e.g., Al on InAs nanowires. In all cases the InAs nanowires have been grown in a molecular beam epitaxy (MBE) system at UCPH whereafter metal films are deposited with different types of in-situ shadow masks. Importantly, the nanowires are kept under UHV throughout the metallization process which enabled a high degree of epitaxial ordering (and chemical cleanliness) at the InAs-metal interface. Electron microscopy characterizations (SEM and TEM) have been performed at UCPH while electrical characterizations are shared between UBAS and UCPH. In this section we report on the in-situ shadowing methods with a brief introduction to geometrical factors that are key for understanding the limitations of the presented shadowing schemes.

Depositing materials from a finite source through a shadow mask always produces regions of partial flux shadowing that connects the fully shadowed region and the non-shadowed part. The length of the region (l_t) depends on several geometrical factors (distances to shadowing object and source, evaporation angle, source diameter) and has been worked out analytically. This length corresponds directly to the transition length from full film coverage to no material deposited for specific materials with a short diffusion length for atom motion on the nanowire surface (depending on the substrate temperature), e.g., Ta and Nb [Carrad (2020)]. For other materials such as Al and Pb the transition length also depends on kinetic and thermodynamical limiting factors [Kanne (2021)]. In all cases this length applies as a geometric limit for the ability for define precise metal patterns by the shadowing scheme.

Two overall approaches for defining in-situ shadows are investigated. The first approach (shown schematically in Fig. 1a,b) utilizes other “as-grown” nanowires as the shadow mask whereas the second approach relies on growth of nanowires on pre-growth fabricated substrate shadow masks (Fig. 1c). In-situ shadows utilizing nanowires can either be enforced by placing a shorter nanowire in front of another (Fig. 1a), or by altering the growth direction of the “masking” nanowire (Fig. 1b). As a direct consequence of the finite transition length, the distance to the shadowing object is limited in order to ensure a full shadow region. For the evaporation system at UCPH the typical maximum distance is around $3\mu\text{m}$ for evaporation of materials with a short diffusion length with a 100nm shadowing object.

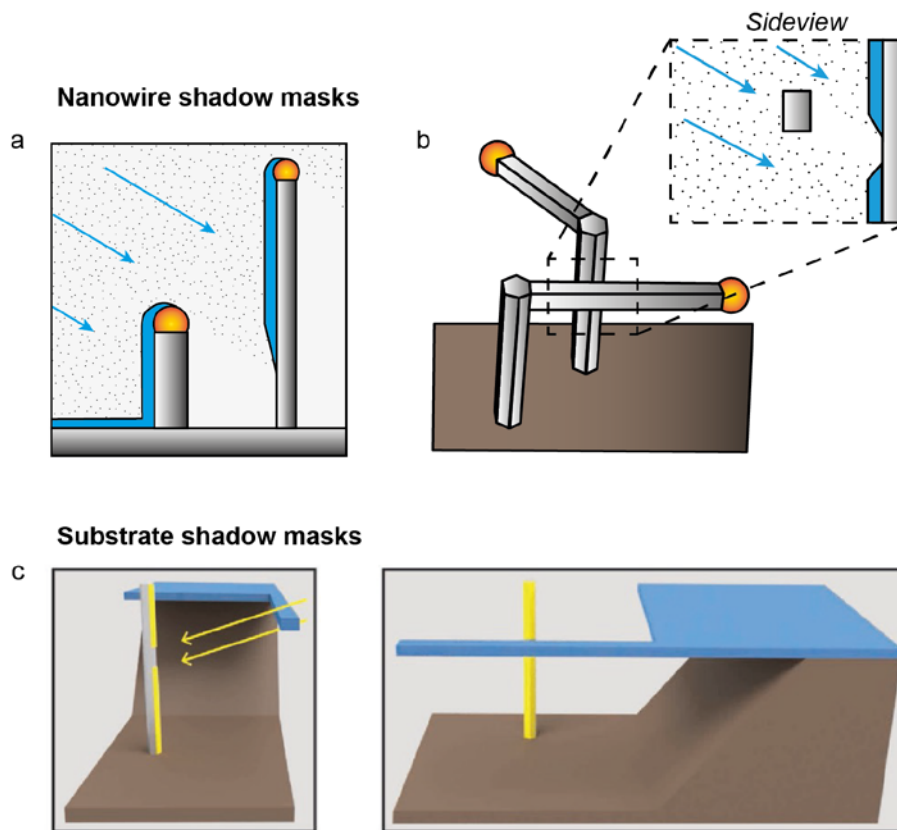


Figure 1: Schematics of two different methods for in-situ shadowing effect on nanowires. a, b In-situ shadowing defined by other as-grown nanowires. **c** Pre-growth fabricated substrates are utilized as a shadow mask.

The InAs nanowires are grown by the vapor-liquid-solid (VLS) mechanism on InAs (111)B substrates. The nanowires are initially grown along the [0001]B direction with $\{1\bar{1}00\}$ facets and a Wurtzite crystal structure. By introducing a short flux of Ga during the axial nanowire growth step, the growth direction can be altered (Fig. 1b) corresponding to one of the six facets (i.e., along one of the $\langle 1\bar{1}00 \rangle$ directions of the nanowires) [Jespersen (2018)]. By defining the initial Au particles prior to the nanowire growth, we can engineer the catalyst volume and position to fit the desired shadowing scheme. To ensure a short junction in the metal film (for instance utilizing the “kink nanowire” shadow scheme), the Au particles can be positioned as schematically shown in Fig. 2a. Here a metal film is deposited with a shallow angle ($\sim 10^\circ - 20^\circ$) along one of the six $\langle 1\bar{1}0 \rangle$ directions of the substrate (highlighted with the blue arrow). By positioning the front nanowire a distance d_1 in front of the target nanowire and a distance d_2 to the side, three of the six growth directions will result in a shadow on the targeted nanowire. By adjusting the d_1/d_2 parameters we can control the position and the spread of the junctions on the target nanowire. In addition to this, the height of the front nanowire can be engineered by precise tuning of the initial Au volume.

To increase the chance for single junction formation or to enable double junctions in the metal films, multiple nanowires can be placed in front of the back nanowire as shown in Fig. 2b-f. In Fig. 2b we show a single junction and in Fig. 2c (Fig. 2f) we show how a single (double) junction can also be combined with a longer shadow region at the bottom. Here the kinking mechanism is suppressed by increasing the initial Au volume. As mentioned above the spread in the position of the junctions on the targeted nanowire can be controlled by the choice of e.g., d_2 value. In Figs. 2d and 2e we see how a relatively large d_2 (300nm) in combination with different kinking directions in the same initial Au particle design can produce double junctions that are well separated (1 μ m) and close to each other (100nm).

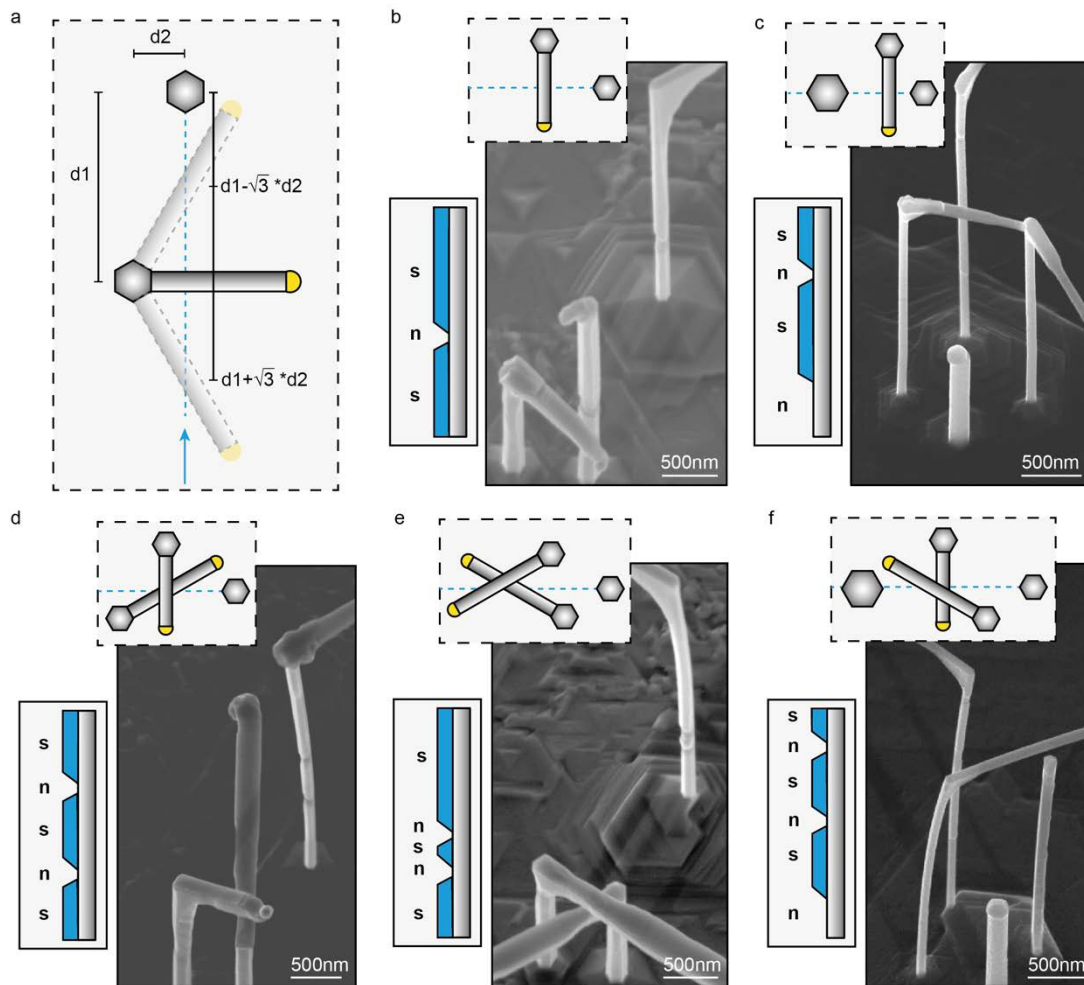


Fig.2. Kinked nanowires used as shadow masks. **a** Topview schematic of the three possible shadowing directions. **b-f** SEM micrographs of kinked InAs nanowires used to define junctions in subsequently deposited Al films.

Following the discussion above, nanowires with a specific junction geometry can be identified either by SEM characterization or by assessing the kinking direction in an optical microscope. To transfer the nanowires to a device relevant substrate a micromanipulator needle setup is used. However, without the ability to engineer the kinking directions, single nanowire junctions using one shadowing nanowire cannot reach a yield of more than 50%. By utilizing two shadowing nanowires the maximum yield for at least one junction increases (to 75%) with 25% chance of double junctions. If a specific distance between double shadow junctions is required, the yield is reduced (down to one out of 36 attempts). In addition to this, with this method it is difficult to form shadow junctions in full shell nanowires.

A reliable method of producing precisely engineered shadow defined junctions in Al films on InAs nanowires was developed based on growth of nanowires on InAs substrates with pre-growth fabricated substrate shadow masks (the strategy shown in Fig. 1c). To fabricate the substrate shadow masks, SiO_x is initially deposited on epi-ready InAs (111)B substrates and patterned by standard electron-beam lithography (EBL). The SiO_x films are then selectively etched in a buffered HF solution followed by a selective InAs wet etching procedure [Carrad (2020)]. A false-colored SEM micrograph of a bare substrate shadow wafer (before growth) is shown as an inset in Fig. 3a. In this approach, the subsequently deposited material is deposited from a direction parallel to the trenches and inclined by an appropriate angle following the discussion above. The bridge design is thereby projected as a pattern in the superconducting layer on each nanowire. With this technique we can form long shadows at the bottom of the nanowires (Fig. 3c), single junctions (Fig. 3d) or multiple junctions (Fig. 3e). We can furthermore ensure nanowires with identical shadow masked junction lengths and with distances in between junctions that are determined by the mask design and the evaporation

conditions. However, making shadow junctions utilizing the substrate shadowing scheme relies on the precision and dimensions of the mask features.

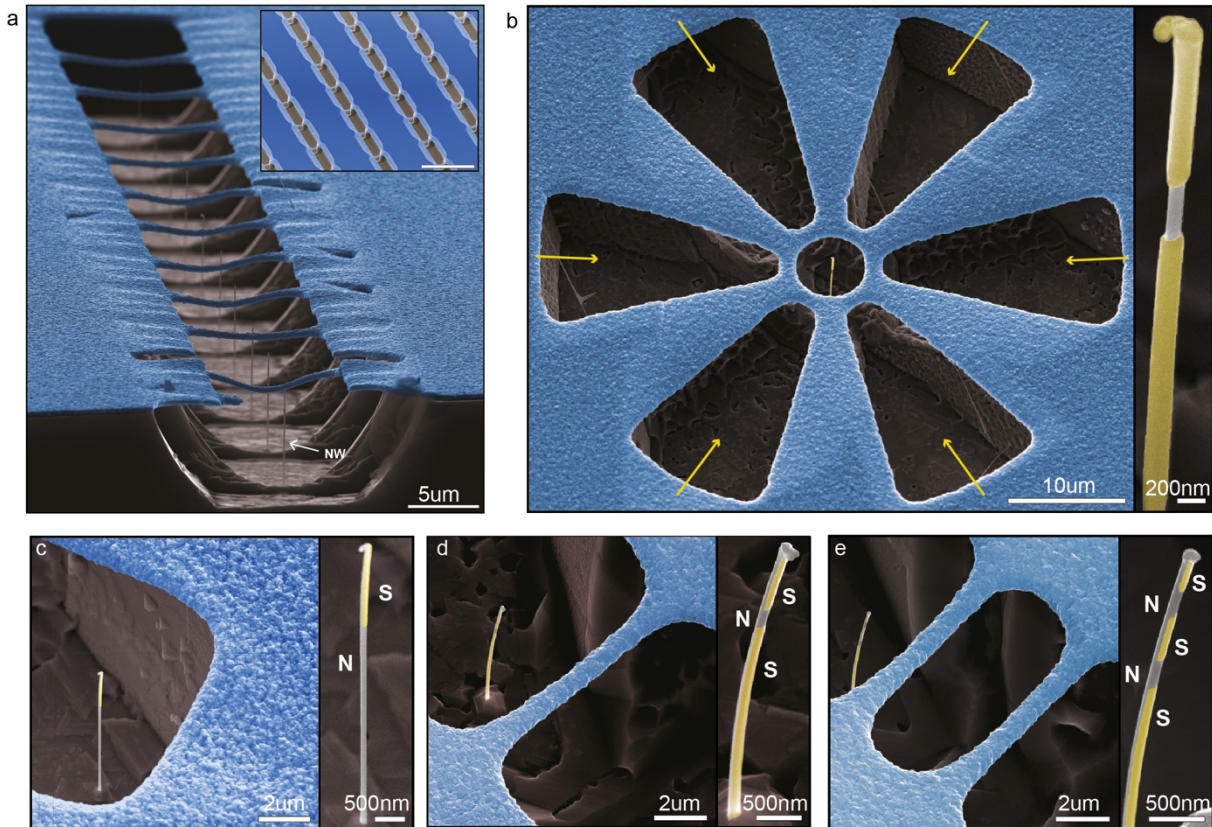


Fig. 3: Substrate shadow masks. False-color SEM micrographs of SiO_x (blue) bridges spanning over trenches in InAs (gray) substrates, from Ref. [Carrad (2020)]. InAs NWs are grown in proximity to the bridges, which act as a shadow mask. **b** Six depositions of $\sim 10\text{nm}$ were performed with 60° rotations according to the openings in the mask (indicated by yellow arrows). **a, c-e** single side evaporation of $\sim 20\text{nm}$ Al.

In conclusion, we have demonstrated two schemes for manufacturing nanowires with single and double shadow junctions. While the focus here is on realizing resistless junctions in thin Al films on InAs nanowires the presented shadowing schemes are equally applicable for any nanowire-metal/insulator combination (additional examples are provided in [Carrad (2020)]). This may in the future extend the scope to other applications utilizing superconducting films with for instance weak etch selectivity or to other systems where pristine surfaces and interfaces are key. The schemes are likewise applicable to other MBE grown nanowires, such as InSb or GaAs and even applied in other growth systems such as MOCVD or CBE.

3. Electrical characterization of few-mode junctions

Having established that single and double “shadow” junctions in Al films on InAs nanowires can readily be defined, with some degree of control of the morphology, dimensions and positions of the junctions, we turn to investigating their electrical properties. We focus on two devices with lengths around 100nm and 350nm, respectively, using nanowires from different MBE growth runs. In both devices the junctions were made using the nanowire-shadow approach.

In the first device we show junctions formed by nanowires grown under normal kinked InAs nanowire growth conditions which generally showed junction lengths from 50-200nm (see histogram in Fig. 4b extracted from SEM characterization of 83 nanowires). Here the spread in junction lengths relates to the controlled variations of the initial Au volume of the catalyst particle, i.e., the diameter of the nanowires. Nanowires nucleated from the smallest defined initial Au volumes generally give junctions in the range of 60-100nm. In the second device, the kinked InAs nanowires were overgrown with InAs prior to metal evaporation. This last step increased the size of the shadowing nanowire and thus increased the junction lengths. Both devices are characterized by voltage biased transport spectroscopy, measuring the two-terminal conductance as a

function of gate and bias voltages. The transport measurements were carried out at temperatures above the critical temperature ($\sim 2\text{K}$), i.e., in the normal state, in order to identify signatures of ballistic transport. The nanowires were transferred to the substrate by micromanipulation and contacted by standard EBL, where source/drain electrodes were attached to the Al shells.

Figure 4 shows transport measurements of a device with a 100nm junction (see inset in Fig. 4a) formed in a 20nm Al film. The zero-field linear conductance trace (Fig. 4c) has indications of a plateau around $2e^2/h$ as expected for a single 1D ballistic channel albeit with a superimposed resonance peak. The resonance appears weakened at 1T and at high field (5T) the $2e^2/h$ plateau is flat. At the high field we see the e^2/h plateau arising due to Zeeman splitting of the 1D subbands. More substantial evidence of ballistic transport can be found in non-linear transport spectroscopy, Fig. 4d-f. These so-called waterfall plots show differential conductance as function of source drain bias and electrostatic gating for 0T (Fig. 4d), 1T (Fig. 4e) and 5T (Fig. 4f) applied parallel to nanowire. In Fig. 4d and 4e we again observe the main plateaus at multiples of $2e^2/h$ at zero bias but also half-plateaus (e^2/h) at finite V_{sd} , when the bias matches the 1D subband spacing. At high field all main and half-plateaus are clearly defined in this regime, holding 1-2 spin polarized transmitting modes (Fig. 4f). While the conductance is not perfectly quantized, the InAs nanowire shadowed junction shows signatures of ballistic transport even at zero field, which is improved upon application of a magnetic field consistent with other works on shadow junctions, e.g. [Khan (2020)].

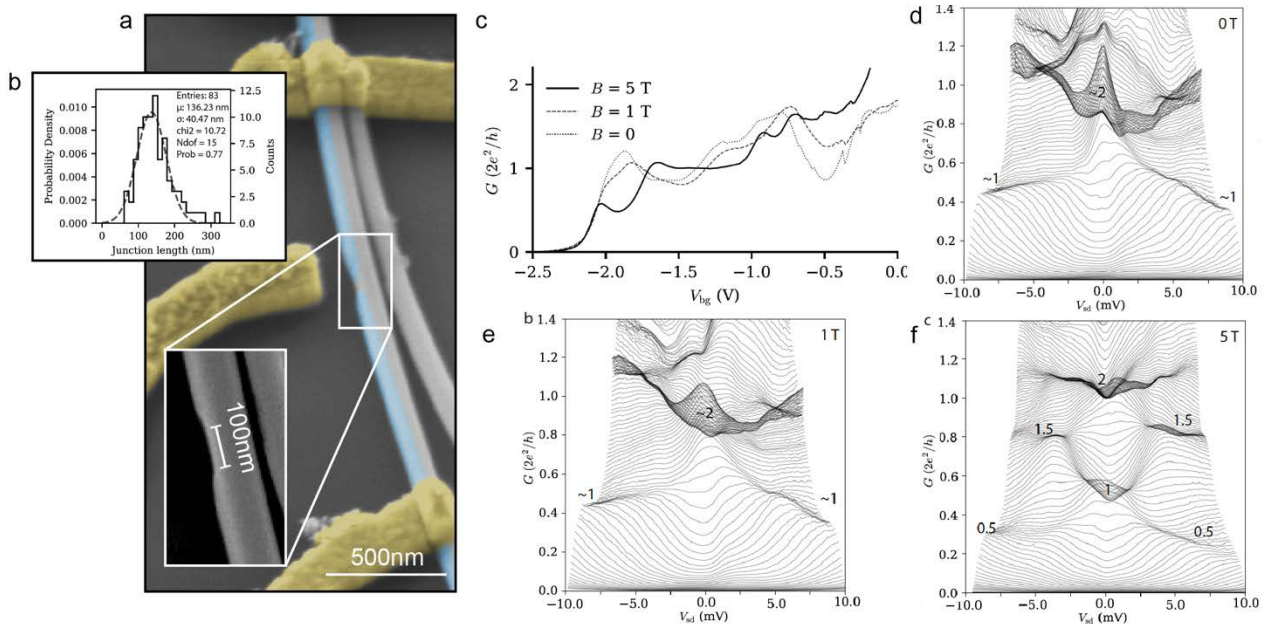


Fig. 4: Electrical measurements of a short Al junction $\sim 100\text{nm}$. *a* SEM micrograph of the device (the second nanowire is not connecting the two electrodes). *b* Junction length distribution fitted with a gaussian distribution centered around 136nm. *c* Differential conductance as function of backgate voltage for 0T, 1T and 5T field applied parallel to the nanowire axis. *d-f* Differential conductance as function of backgate voltage and source-drain bias for 0T(*d*), 1T(*e*) and 5T(*f*). All measurements were performed at 2K.

In Fig. 5 we show transport measurements from a device with a 350nm junction (see inset in Fig. 5b) in a 28nm Al film. A SEM micrograph of the InAs/Al nanowire before transfer is shown in Fig. 5a. As evident from the linear conductance trace (Fig. 5c), the extended junction region gives rise to more resonances and hence the $2e^2/h$ plateau is less clearly defined (at zero field) compared to the shorter junction in Fig. 4. At increased field (1T) the $2e^2/h$ plateau appears more pronounced and at 5T a long e^2/h plateau is visible. Similarly, from the waterfall plots, Fig. 5e (0T,1T), a sign of bunching of the conductance lines is observed at zero bias around $2e^2/h$, however, resonances are also abundant. At high field (5T) resonances are suppressed, yielding a clearer indication of quantized conductance. We note that conductance quantization is not observed at higher gate voltages (not shown) consistent with the relatively long junction length (compared to expected mean free path).

Finally, in Fig. 5d, we demonstrate fabrication of a superconducting quantum interference device (SQUID) implemented on a double Josephson junction nanowire (with junction lengths $\sim 250\text{nm}/250\text{nm}$), utilizing the

two closely separated junctions in the Al film caused by the kinked nanowire shadows (see Fig. 2e). While this type of devices is still to be investigated in detail, the double junctions are expected to be of similar quality as the single junction devices. The double Josephson junction SQUID design additionally allows for indirect probing of Andreev bound state via the current phase relation (complementary approach to evaluate the junction transmissions). Furthermore, the device geometry can be altered, e.g. into the multi-qubit architecture outlined in the AndQC proposal.

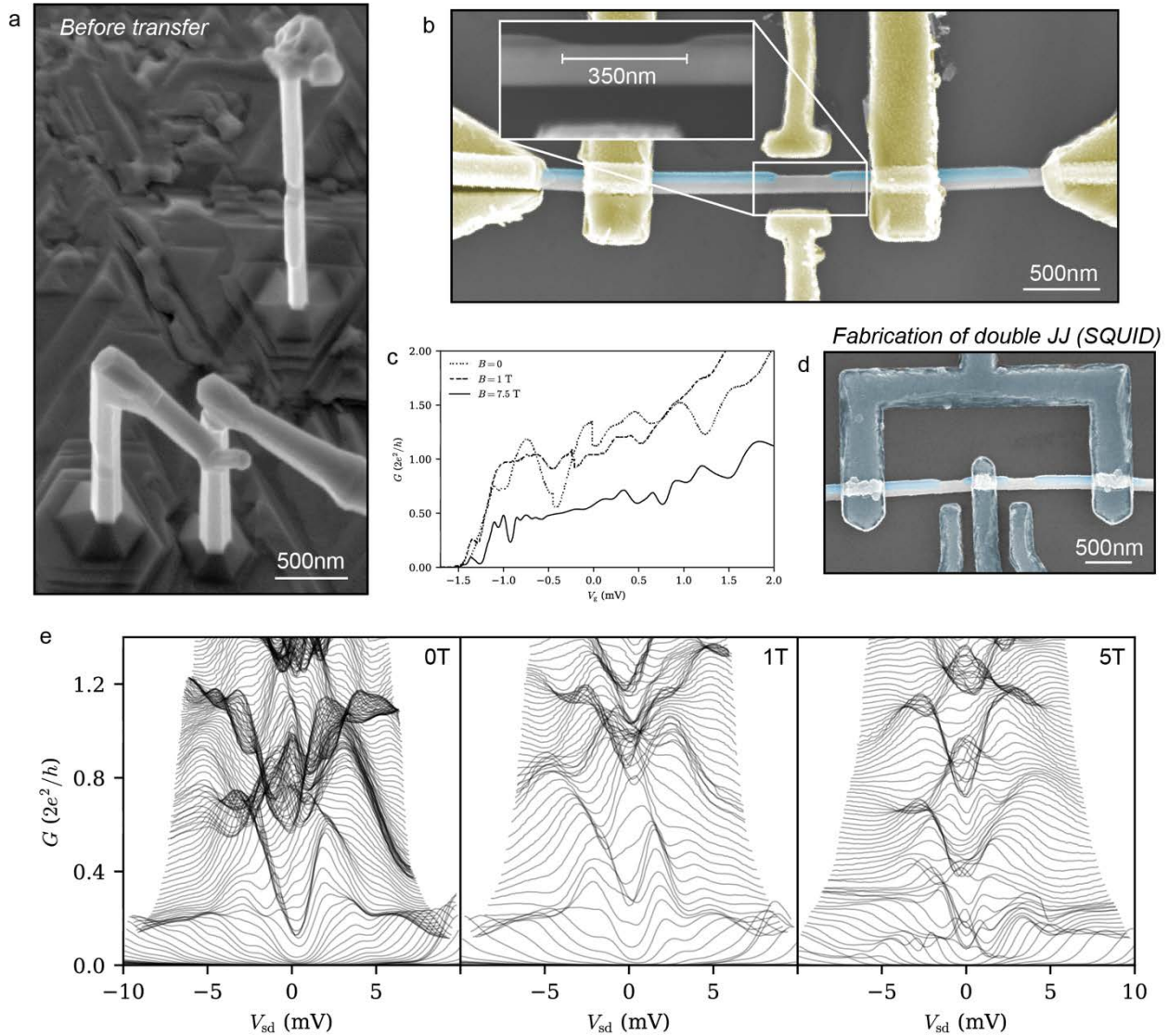


Fig. 5: Electrical measurements of a long Al junction ~ 350 nm. **a** SEM micrograph of the nanowire used for the device shown in **b**. **c** Differential conductance as function of backgate voltage for 0T, 1T and 7.5T. **d** SEM micrograph of a double junction nanowires device used in a superconducting quantum interference device geometry. **e** Differential conductance as function of backgate voltage and source-drain bias for 0T(left), 1T(middle) and 5T(right). All measurements are taken at 2K.

4. Implementation of superconducting junctions in cavities

The group at UBAS has successfully contacted and characterized several shadow-epitaxy Al/InAs nanowire junctions. Using a micromanipulator, the nanowires were deterministically placed on a Si substrate and the junctions were identified by means of scanning electron microscopy. They could be contacted with both sputtered NbTiN and evaporated Al after removing the native oxide by in-situ Ar-milling. Out of in total 11 characterized junctions, 10 exhibited a gate-tunable current, making them a highly reproducible platform.

Furthermore, fabrication is simplified compared to conventional Al/InAs junctions that are defined by a wet-etch technology.

Given the high reproducibility, we have integrated the shadow-epitaxy junctions in a circuit quantum-electrodynamics architecture. We have realized a quarter-wave resonator based on NbTiN that can be seen in Fig 6a. The scanning electron micrograph in Fig. 6b shows the shadow-epitaxy Al/InAs nanowire which is embedded in an Al loop that shunts the current anti-node of the resonator (see inset in Fig 6b). The charge carrier density in the junction and the lead can be individually addressed by two side gates. The resonator in the integrated system has a resonance frequency of 6.428 GHz and a loaded quality factor of 700. Fig. 6c shows a spectroscopy plot for the resonator. As a function of gate voltage, we observe two avoided crossings. Similar crossings are also observed as a function of flux in the nanowire-loop (Fig 6d) indicating that the crossing transitions originate from Andreev levels in the Josephson junction. Furthermore, we perform two-tone spectroscopy to measure the dispersion of the crossing level transitions. We observe a finite dispersion as a function of both gate voltage and flux (Fig 6e and 6f). The smallest observed transition frequency is approximately 5 GHz indicating, under the assumption of a short junction model, the presence of highly transparent channels in the shadow-epitaxy Josephson link.

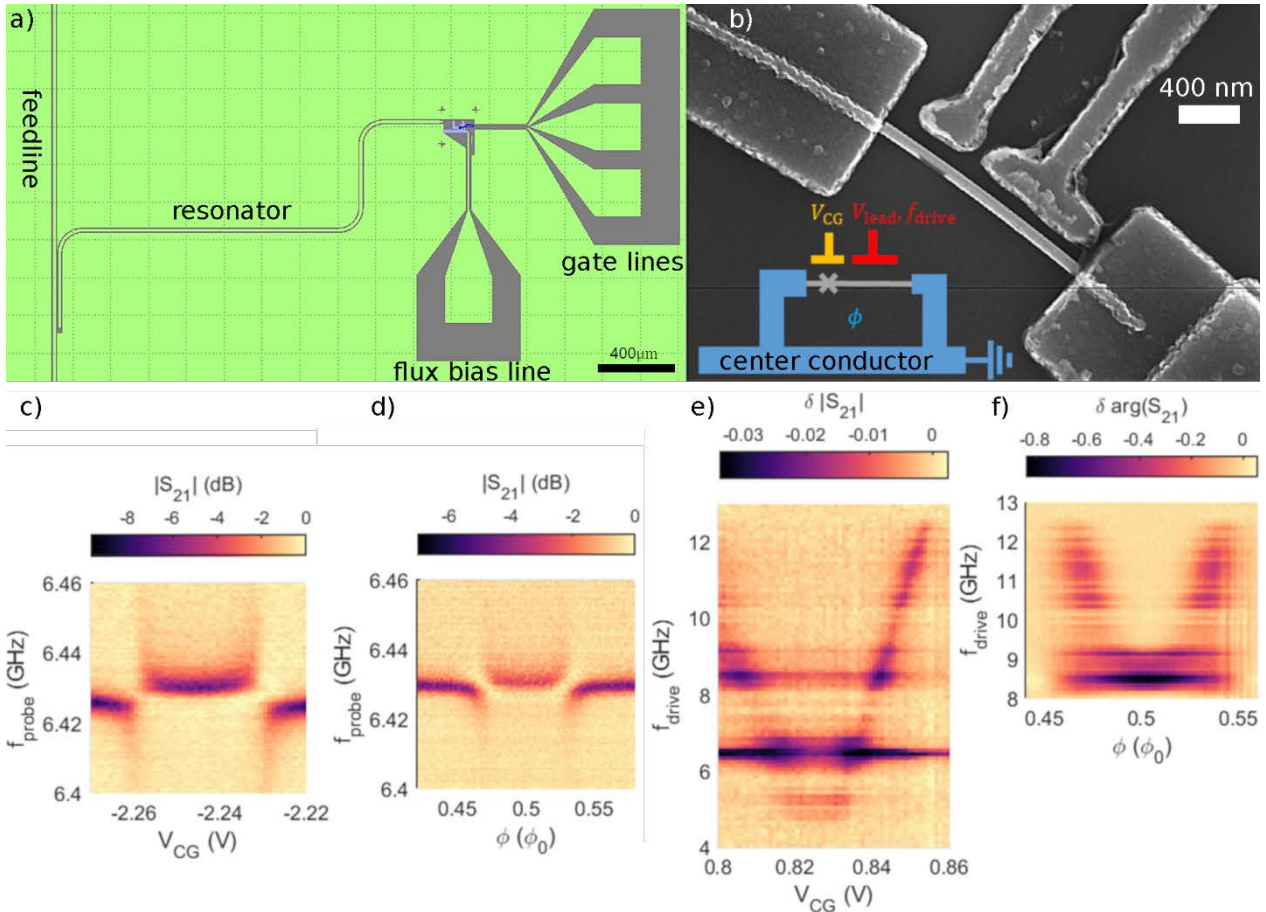


Fig. 6: Integration of an Al junction in a superconducting cavity. *a* Schematic of the superconducting resonator. *b* Scanning electron micrograph of the device. The clearly visible shadow-epitaxy junction is contacted with Al leads. *c* Transmission through the feedline as a function of gate voltage exhibiting an anti-crossing. *d* Same as *c*, but as a function of flux. *e* Two-tone spectroscopy of the level transition that crossed the resonator in *c* and *d* as a function of gate voltage. *f* Same as *e* but as a function of flux.

5. Conclusion

In conclusion we have demonstrated two methods for making in-situ shadow junction in metal films on InAs nanowires. We discussed geometric limiting factors for the presented schemes and showed how these were utilized to make well defined single and double junctions with varied dimensions. From transport measurements, the shadowed defined junctions were shown to facilitate a high yield of functional devices where 10 out of 11 measured exhibited gate-tunable currents. Additionally, we found features of ballistic transport in shadow defined devices and that these signatures were less significant for longer junctions. However, as the strict requirements for the transmission probability ($\tau \geq 0.95$) can be reduced by increasing the junction length, these junctions may be of similar interest in the AndQC project. It is encouraging that clear signatures of ballistic transport are observed in these pure InAs nanowire junctions. Earlier demonstrations of ballistic behavior were reported in higher mobility materials such as Sb-based nanowires, e.g., Refs. [Khan (2020), Zhang (2017), Estrada (2018)].

The observations of few mode transport and ballistic behavior in the InAs are matching the standards of the field [Khan (2020), Zhang (2017), Estrada (2018)]. We note that superconducting island devices defined by the substrate shadowing technique have also shown superior characteristics in terms of stability as shown in our Ref. [Carrad (2020)]. This paper discusses in more details the advantages of shadow epitaxy for normal-superconductor junctions and superconducting island devices, while we have focused here mainly on the Josephson junction geometry relevant for AndQC. It has been demonstrated by UBAS that the shadow Josephson junctions can indeed be embedded in superconducting circuits with the smallest observed transition frequency indicating highly transparent channels.

References

- [Krogstrup (2015)] Krogstrup, P., N.L.B. Ziino, W. Chang, S.M. Albrecht, M.H. Madsen, Erik Johnson, J. Nygård, C.M. Marcus, and T.S. Jespersen. 2015. "Epitaxy of Semiconductor-Superconductor Nanowires." *Nature Materials* 14 (4): 400–406.
- [Chang (2015)] Chang, W., S. M. Albrecht, T. S. Jespersen, F. Kuemmeth, P. Krogstrup, J. Nygård, and C. M. Marcus. 2015. "Hard Gap in Epitaxial Semiconductor–superconductor Nanowires." *Nature Nanotechnology* 10 (3): 232–36.
- [Carrad (2020)] Carrad, Damon J., Martin Bjergfelt, Thomas Kanne, Martin Aagesen, Filip Krizek, Elisabetta M. Fiordaliso, Erik Johnson, Jesper Nygård, and Thomas Sand Jespersen. 2020. "Shadow Epitaxy for In Situ Growth of Generic Semiconductor/Superconductor Hybrids." *Advanced Materials* 32 (23): 1908411.
- [Kanne (2021)] Kanne, Thomas, Mikelis Marnauza, Dags Olsteins, Damon J. Carrad, Joachim E. Sestoft, Joeri de Bruijckere, Lunjie Zeng, Erik Johnson, Eva Olsson, and Kasper Grove-Rasmussen. 2021. "Epitaxial Pb on InAs Nanowires for Quantum Devices." *Nature Nanotechnology* 16 (7): 776–81.
- [Jespersen (2018)] Jespersen, T. S., P. Krogstrup, A. M. Lunde, R. Tanta, T. Kanne, E. Johnson, and J. Nygård. 2018. "Crystal Orientation Dependence of the Spin-Orbit Coupling in InAs Nanowires." *Physical Review B* 97 (4): 41303.
- [Khan (2020)] Khan, Sabbir A., Charalampos Lampadaris, Ajuan Cui, Lukas Stampfer, Yu Liu, Sebastian J. Pauka, Martin E. Cachaza, Elisabetta Maria Fiordaliso, Jung-Hyun Kang, and Svetlana Korneychuk, Timo Mutas, Joachim E. Sestoft, Filip Krizek, Rawa Tanta, Maja C. Cassidy, Thomas S. Jespersen, and Peter Krogstrup. 2020. "Highly Transparent Gateable Superconducting Shadow Junctions." *ACS Nano* 14 (11): 14605–15.
- [Zhang (2017)] Zhang, Hao, Önder Gül, Sonia Conesa-Boj, Michał P. Nowak, Michael Wimmer, Kun Zuo, Vincent Mourik, Folkert K. de Vries, Jasper van Veen, and Michiel W. A. de Moor, Jouri D. S. Bommer, David J. van Woerkom, Diana Car, Sébastien R Plissard, Erik P.A.M. Bakkers, Marina Quintero-Pérez, Maja C. Cassidy, Sebastian Koelling, Srijit Goswami, Kenji Watanabe, Takashi Taniguchi & Leo P. Kouwenhoven. 2017. "Ballistic Superconductivity in Semiconductor Nanowires." *Nature Communications* 8 (1): 16025–16025.

[Estrada (2018)] Saldaña, Juan Carlos Estrada, Yann Michel Niquet, Jean Pierre Cleuziou, Eduardo J.H. Lee, Diana Car, Sébastien R. Plissard, Erik P.A.M. Bakkers, and Silvano De Franceschi. 2018. "Split-Channel Ballistic Transport in an InSb Nanowire." *Nano Letters* 18 (4): 2282–87.